NASA Contractor Report 191415

ICASE Report No. 92–74

IN-64
158527
P.38

ICASE

ON ESSENTIALLY NON-OSCILLATORY SCHEMES ON UNSTRUCTURED MESHES: ANALYSIS AND IMPLEMENTATION

(NASA-CR-191415) ON ESSENTIALLY NON-OSCILLATORY SCHEMES ON UNSTRUCTURED MESHES: ANALYSIS AND IMPLEMENTATION Final Report (ICASE) 38 p
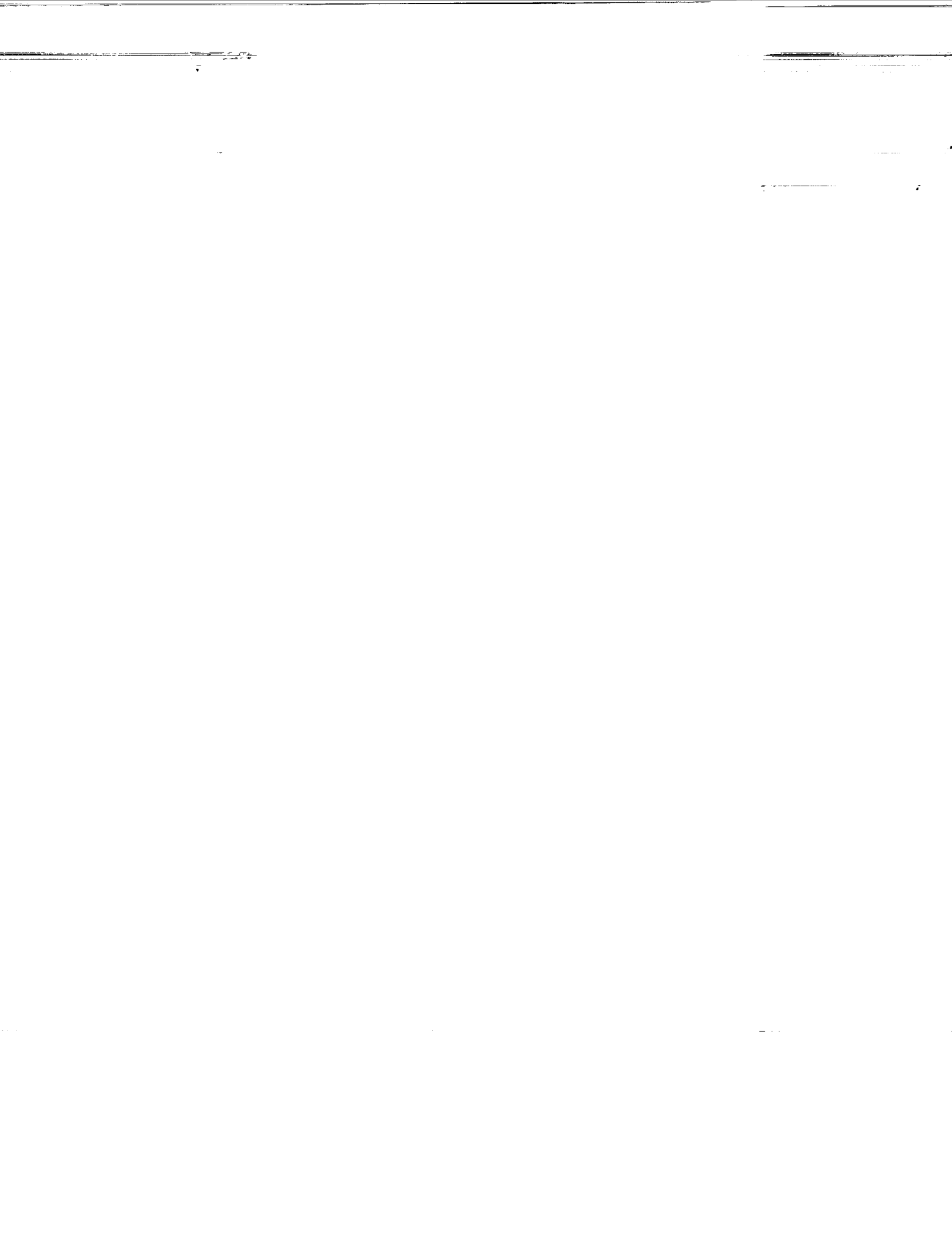
N93-24492

Unclas

G3/64 0158527

R. Abgrall

NASA

National Aeronautics and
Space Administration

Langley Research Center
Hampton, Virginia 23665-5225

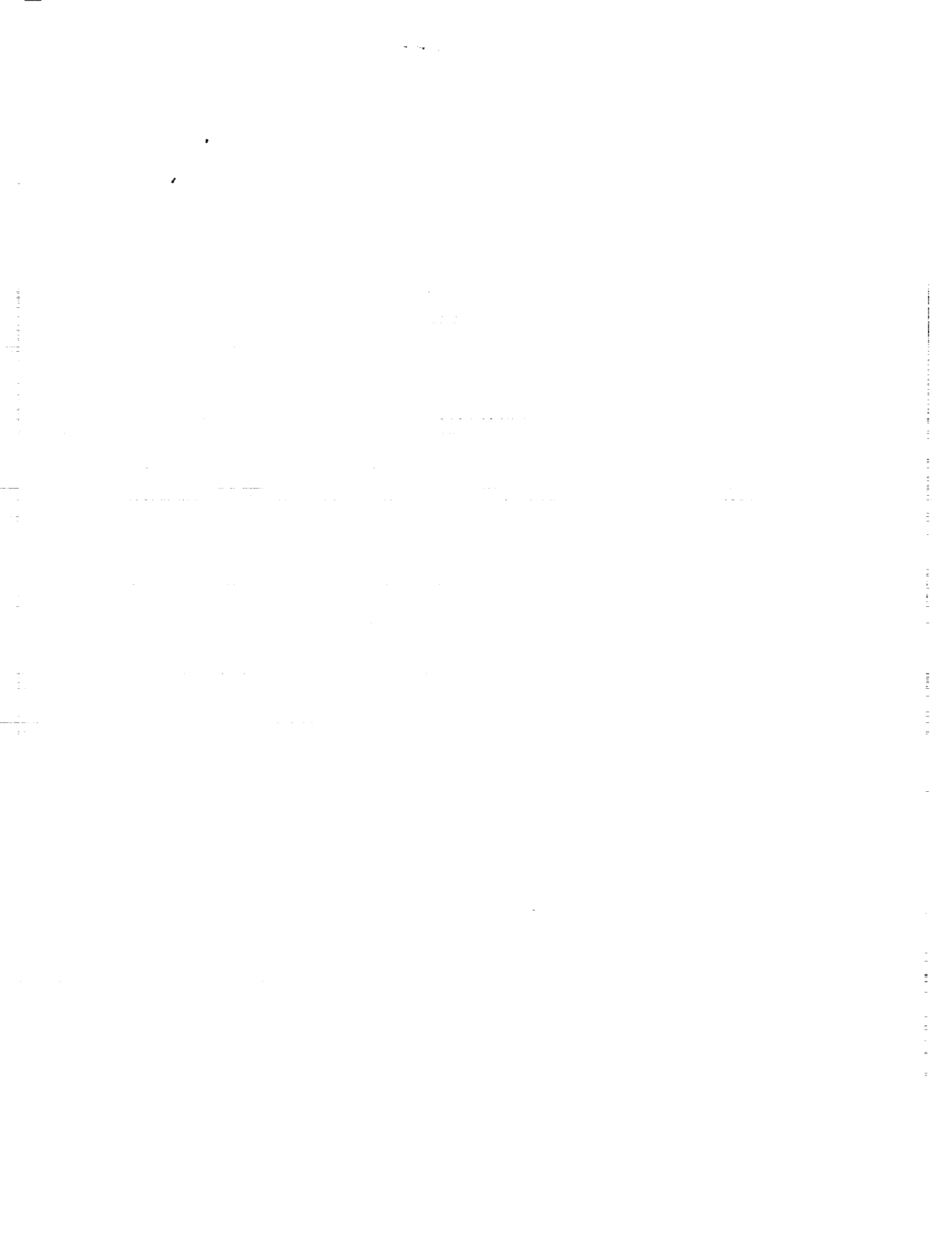# ON ESSENTIALLY NON-OSCILLATORY SCHEMES ON UNSTRUCTURED MESHES: ANALYSIS AND IMPLEMENTATION

R. Abgrall[1]

INRIA, 2004, route des Lucioles

Sophia Antipolis

06560 Valbonne

FRANCE

ABSTRACT

A few years ago, the class of Essentially Non-Oscillatory Schemes for the numerical simulation of hyperbolic equations and systems was constructed. Since then, some extensions have been made to multidimensional simulations of compressible flows, mainly in the context of very regular structured meshes. In this paper, we first recall and improve the results of an earlier paper about non-oscillatory reconstruction on unstructured meshes, emphasising the effective calculation of the reconstruction. Then we describe a class of numerical schemes on unstructured meshes and give some applications for its third order version. This demonstrates that a higher order of accuracy is indeed obtained, even on very irregular meshes.

1 Introduction

During the past few years, a growing interest has emerged in building high order accurate and robust schemes for compressible flow simulation. One of the difficulties is the appearance of possibly strong discontinuities that may interact together, even for smooth initial data. One way to avoid this difficulty is to use a Totally Variation Diminishing scheme. Such a scheme has the property, at least for 1D scalar equations, of not creating new extrema, and hence provides a reasonable treatment of discontinuities. TVD schemes have since been successfully and widely used with many types of meshes (see for example [1] for a review, and among many others [2] for simulations on finite elements type meshes). Nevertheless, one of their main weakness is that the order of accuracy falls to first order in regions of discontinuity and at extrema, leading to excessive numerical dissipation.

Various methods have been proposed to overcome this difficulty (for example, mesh adaptation [3, 4, 5]), but one promising approach may be the class of Essentially Non-Oscillatory schemes (E.N.O., for short), introduced by Harten, Osher and others [6, 7, 8, 9, 10]. The basic idea of E.N.O. schemes is to use a Lagrange type interpolation with an adapted stencil: when a discontinuity is detected, the procedure looks for the region around this discontinuity where the function is the smoothest. This reconstruction technique may be applied either to the node values [9] or to specially constructed averages over control volumes [6, 7, 8]. In the latter case, the approximation is done in a conservative way. This enables approximation of any piecewise smooth function to any desired order of accuracy.

Until now, very few attempts have been made to adapt these ideas to multidimensional flows (see for example [9, 11]), to smoothly varying grids, or especially to unstructured grids. For the latter topic, only preliminary work exists (see [12, 13, 14, 15]). In [14] general ideas were presented with a review of the existing ENO methods, but no implementation was given. In [15] several algorithms were presented and tested on simple problems (linear advection, Burger's like equations), but their reconstruction algorithms appears to be very complicated and costly. There was no study of the numerical stability of the reconstruction. Our experience has shown that this point is fundamental. In [12] we studied two reconstruction methods based on two different polynomial approximations, and have also estimated the behavior of their leading coefficients. This enabled us to design an algorithm that has been shown to give third and fourth order approximation. We also discussed the choice of candidate stencils: a few stencils suffice. In [13] this reconstruction method was implemented for compressible flows problems and tested on a 2D shock tube problem on a triangular mesh. In the finite volume scheme used, the control volumes were the triangles of the mesh. If one wants this set to be as isotropic as possible, the minimum number of

possible stencils is much larger than in the version presented in [12]; its construction is also less natural. This makes the scheme of [13] very costly.

This paper is organized as follows. In section 2 we recall and improve the results obtained in [12]. These results are valid whatever the type of the underlying mesh (structured or not). In particular, we pay much attention to the study of the numerical stability of the reconstruction algorithm. In section 3 we present our numerical scheme. In section 4 some numerical results are presented. Finally, several general comments are made in the conclusion. Throughout this paper, the values used are the average values in the given control volumes.

2 The reconstruction problem on unstructured meshes

Let us first recall basic facts about 1D reconstruction. They show why a new method has to be introduced for unstructured meshes. We first recall how to interpolate data in an essentially non-oscillatory Lagrange fashion, and then how this is used to reconstruct 1D data.

Essentially non-oscillatory interpolation. This relies on two well known properties of divided differences. Let $\{y_0 \leq y_1 \leq \ldots \leq y_k\}$ be a stencil, and let $[y_0, \ldots y_k] v$ be the $k+1^{th}$ divided difference of v, a piecewise smooth real valued function.

(i) If v is $p \geq n$ times continuously differentiable in the interval $[y_0, y_k]$, then

$$[y_0, \ldots y_k,] v = \frac{f^{(k)}(\xi)}{k!} + O(|y_k - y_0|^{n-k}) \quad \text{for all } k \leq n \text{ and some } \xi \in [y_0, y_k].$$

(ii) If $v^{(p)}$, $p \leq n$, admits a jump $[v^{(p)}]$ in $[y_0, y_k]$, then

$$[y_0, \ldots y_k] v = O\left(\frac{[v^{(p)}]}{|y_k - y_0|^{k-p}}\right) \quad \text{for all } k, \ p+1 \leq k \leq n.$$

These relations show that the divided differences remain bounded whatever the mesh size, for smooth functions, but go to infinity rather quickly for nonsmooth functions. With the help of these two remarks, Harten et. al. have derived the following E.N.O. interpolation algorithm: Assume a grid $\{y_j\}, y_j < y_{j+1}$. For any j, first consider $\mathcal{S}^{(0)} = \{y_j\}$.

(i) If $|[y_j, y_{j+1}]v| < |[y_{j-1}, y_j]v|$ then $\mathcal{S}^{(1)} = \{y_j, y_{j+1}\}$, else $\mathcal{S}^{(1)} = \{y_{j-1}, y_j\}$.

(ii) Assume that $\mathcal{S}^{(k)} = \{y_{j_0}, \cdots, y_{j_k}\}$, a stencil for $k+1^{th}$ order reconstruction, is given (y_{j_0} and y_{j_k} are the extreme points of the stencil). If $|[y_{j_0-1}, y_{j_0}, \ldots, y_k]v| < |[y_{j_0}, \ldots y_{j_k}, y_{j_k+1}]v|$ then $\mathcal{S}^{(k+1)} = \mathcal{S}^{(k)} \bigcup \{y_{j_0-1}\}$, else $\mathcal{S}^{(k+1)} = \mathcal{S}^{(k)} \bigcup \{y_{j_k+1}\}$.

Once the required number of points has been chosen, one can compute Lagrange interpolation based on the last stencil of the algorithm: this is the E.N.O. interpolation of v.

The 1D conservative reconstruction. We consider a mesh on $\mathbb{R}$, $\{x_i\}_{i \in \mathbb{Z}}$, that may or may not be regular. Around each point, x_i, we define a control volume $[x_{i-1/2}, x_{i+1/2}]$ where as usual,

$$x_{i+1/2} = \frac{x_i + x_{i+1}}{2}.$$

Let us consider u, a piecewise smooth real valued function. We let $\overline{u}_i$ denote the average of u in $[x_{i-1/2}, x_{i+1/2}]$:

$$\overline{u}_i = \frac{1}{x_{i+1/2} - x_{i-1/2}} \int_{x_{i-1/2}}^{x_{i+1/2}} u(t) \, dt \tag{1}$$

There are two classical ways of reconstructing u from its averages:

(i) **Reconstruction via primitive functions.** One considers W a primitive of u, say

$$W(x) = \int_{x_{1/2}}^{x} u(t) \, dt.$$

The values of W at the points $x_{j+1/2}$ are easily recovered from the data:

$$W(x_{i+1/2}) = \sum_{j=0}^{j} (x_{i+1/2} - x_{i-1/2})\overline{u}_i$$

One computes an essentially non-oscillatory reconstruction $R(W, n+1)$ of W, up to the order $n+1$, as explained above. Here, one sets $y_j = x_{j+1/2}$. The reconstruction of u, $R(u, n)$ is defined as:

$$R(u, n) = \frac{dR(W, n+1)}{dx}$$

Clearly the average values of $R(u, n)$ over any $[x_{i-1/2}, x_{i+1/2}]$ is $\overline{u}_i$.

(ii) **Reconstruction via deconvolution.** Here, the mesh *must* be regular, $x_{i+1/2} - x_{i-1/2} = \Delta x$. One may see equation (1) as the convolution product v of u and the characteristic function of $[-\Delta x/2, \Delta x/2]$. One has $v(x_i) = \overline{u}_i$. Then v is reconstructed in an essentially non-oscillatory fashion as explained above, where $y_j = x_j$. Finally, one applies a deconvolution operator to $R(v, n)$, as in [6] for example, to get $R(u, n)$.

3

Atkins & Casper [11] have used a tensor product of 1D-reconstructions to derive their numerical scheme. This is possible because they assume a regular transformation between a Cartesian mesh of $[0, 1] \times [0, 1]$ and their computational grid. The same trick has been used in Shu et. al. [9]. In the context of unstructured grid, these tricks cannot work for at least two reasons:

(i) The reconstruction via deconvolution needs very regular meshes (each control volume can be obtained from any other by translation),

(ii) The reconstruction via primitive function methods needs to know point values of a primitive over any *rectangle* on the data. Hence, these rectangles must be exactly covered by control volumes. As can be seen in Figure 1, this is in general impossible.

These two remarks show that a straightforward extension of one dimensional ideas is not sufficient.

2.1 Preliminaries

In the sequel, the symbol $\mathbb{R}_n[X, Y]$ denotes the set of polynomials P in the variables X and Y of total degree less than or equal to n:

$$P(X, Y) = \sum_{l=1}^{n} \sum_{i+j=l} a_{ij} X^i Y^j$$

The set $\mathbb{R}_n[X, Y]$ is a vector space of dimension $N(n) = \frac{(n+1)(n+2)}{2}$, a basis of which is the set of monomials

$$\left\{ (X - x_0)^i (Y - y_0)^j \right\}_{i+j \leq n}$$

where (x_0, y_0) is any point of $\mathbb{R}^2$. The total degree of P does not depend on the choice of (x_0, y_0). As we will show later, this kind of basis is not the best suited for practical calculations.

Let $\mathcal{M}$ be a mesh of the finite element type. Associated with this mesh, we have a triangulation $\mathcal{T}$. We may consider several kind of control volumes, for example the triangles of $\mathcal{T}$ themselves or the dual mesh (see Figure 2). The dual mesh are constructed as follows: for each vertex M_i, the control volume is obtained by connecting the midpoints of the edges incident on it to the barycenters of the surrounding triangles to which it belongs. Let us denote by $\{C_i\}$ the set of control volumes. We only require the following properties:

• For any $i \neq j$, $C_i \bigcap C_j$ is of empty interior,

4

- C_i is connected,

- There is an algebraic dependency of the C_i's on the points of $\mathcal{M}$ (This is true for the two above examples).

- The boundary of C_i is a locally regular curve (This is also true for the two above examples).

We consider the following problem (problem $\mathcal{P}$ or approximation in the mean for short):

Let u be a regular enough function (say in L^1). Given N and n two integers, a set of control volumes $\mathcal{S} = \{C_{i_l}\}_{1 \leq l \leq N}$, find an element $P \in \mathbb{R}_n[X,Y]$ such that for $1 \leq l \leq N$,

$$< u >_{C_{i_l}} \stackrel{def}{=} \frac{\int_{C_{i_l}} u \ dx}{area(C_{i_l})} = < P >_{C_{i_l}} \tag{2}$$

For this problem to have a unique solution, one must fulfill two conditions:

- $N = \frac{(n+1)(n+2)}{2} = N(n)$

- The following Vandermonde matrix must be non singular:

$$\mathcal{V} = \left[< X^i Y^j >_{C_{i_l}} \right] \begin{array}{c} i+j \leq n \\ 1 \leq l \leq N \end{array} =$$

$$\begin{bmatrix} 1 & < X >_{C_{i_1}} & < Y >_{C_{i_1}} & \cdots & < X^n >_{C_{i_1}} & < X^{n-1}Y >_{C_{i_1}} & \cdots & < Y^n >_{C_{i_1}} \\ \vdots & \vdots & \vdots & \vdots & \vdots & \vdots & \vdots & \vdots \\ 1 & < X >_{C_{i_N}} & < Y >_{C_{i_N}} & \cdots & < X^n >_{C_{i_N}} & < X^{n-1}Y >_{C_{i_N}} & \cdots & < Y^n >_{C_{i_N}} \end{bmatrix} \tag{3}$$

If $\Delta_{\mathcal{S}} = \det \mathcal{V} \neq 0$, then we say that this stencil is admissible. In that case, there is a unique solution to problem $\mathcal{P}$ that will be denoted by P_u.

A similar problem was first considered by Barth et. al. [16] for smooth functions, then by Harten et. al. [14], Vankeirsblick et. al. [15], and Abgrall [12]. In the three first references [16, 14, 15], the authors consider overdetermined systems for two reasons. First, the problem $\mathcal{P}$ does not always have a unique solution. Second they claim that the condition number of the overdetermined system is better than that of problem $\mathcal{P}$. In [12], the same approach as here was adopted. To support that choice, one must notice, as explained in remark 1, that (3) is generally not singular. Also, the condition number of the linear system depends mainly on the basis used for the polynomial expansion, as shown in section 2.4. For these two reasons, we have preferred this approach, which also has the advantage of simplifying the coding of the global scheme.

Remarks:

(i) We do not know if the admissibility condition admits a geometric interpretation (except for $n = 1$). We do not even know whether there is a systematic way of constructing admissible stencils, as is the case for the Lagrange interpolation [17]. Nevertheless, one may say that, in general, any stencil is admissible: one may consider the equation $\Delta_S = 0$ as an algebraic surface in $\mathbb{R}^{2 \times k}$ for some integer k [2]. This surface is then of empty interior, from a topological point of view, so that if S is not admissible, one only has to change slightly the elements of S for it to become admissible. Nevertheless, the condition number of the linear system may be very bad. We will discuss that point in section 2.4.

(ii) This admissibility condition is independent of the basis chosen for expanding the polynomial P.

2.2   Some general results about approximation in the mean

In this section, we give two results on reconstruction in the mean for a function u, which may or may not be smooth. These results generalize well known properties of the Lagrange interpolation of 1D real valued functions, that have been used as a corner stone by Harten and his coauthors to design an essentially non-oscillatory reconstruction. We have to emphasize that the reconstruction is the mean in *not* directly related to Lagrange reconstruction. Throughout this section, if $S^{(n)}$ is an admissible stencil for degree n, the symbol $K(S^{(n)})$ denotes the convex hull of the union of the elements of $S^{(n)}$.

2.2.1   The case of a smooth function

In [12] we have shown the following result. Its proof follows easily from Ciarlet & Raviart's proof on Lagrange and Hermite interpolation.

Theorem 2.1 *Let S be an admissible (for degree n) stencil of $\mathbb{R}^2$, let h and ρ be respectively the diameter of $K(S)$ and the supremum of the diameters of the circles contained in $K(S)$. Let u be a function that admits everywhere in $K(S)$ an $n + 1^{th}$ derivative $D^{n+1}u$ with*

$$M_{n+1} = sup\{\|D^{n+1}u(x)\|;\ x \in K(S)\} < +\infty.$$

If P_u is the solution of problem $\mathcal{P}$, then for any integer m, $0 \le m \le n$,

$$sup\{\|D^m u(x) - D^m P_u(x)\|;\ x \in K(S)\} \le C M_{n+1} \frac{h^{n+1}}{\rho^m}$$

---

[2]because we have assumed an algebraic dependency of the control volumes in terms of the points of $\mathcal{M}$

6

for some constant $C = C(m, n, \mathcal{S})$. Moreover, if $\mathcal{S}'$ is obtained from $\mathcal{S}$ by an affine transformation, that is there exists $x_0 \in \mathbb{R}^2$ and an invertible matrix A such that

$$C'_k \in \mathcal{S}' \quad \text{iff there exists} \quad C_k \in \mathcal{S} \text{ such that } C'_k = A\, C_k + x_0 \quad),$$

then

$$C(n, m, \mathcal{S}) = C(n, m, \mathcal{S}').$$

This result basically states that if the stencil $\mathcal{S}$ is not too flat, *i.e.* the ratio h/ρ is not too large, then P_u will be a good approximation of u. Let us turn now to the case of nonsmooth functions.

2.3 The case of a nonsmooth function

We only discuss the case of piecewise smooth functions. This class is large enough for our purpose. To do the analysis we have to introduce the following property which prevents geometrical degeneration:

Property 2.2 *Let us give $\epsilon > 0$. The admissible stencil $\mathcal{S}^{(n)}$ belongs to $\mathcal{P}_\epsilon^n$ if and only if: for any vector U whose components are zeroes and ones and both values are represented, and for P the nth order polynomial defined by*

$$< P >_{C_{i_j}} = U_j, \quad \text{for all } C_{i_j} \in \mathcal{S}^{(n)},$$

the following property holds: the sum of the absolute value of the n-th order coefficients of P is greater or equal to ϵ, that is

$$\sum_{l=N(n-1)+1}^{N(n)} \left| \frac{det(R_0 \cdots R_{N(n-1)} \cdots \widehat{R}_l \cdots R_{N(n)})}{det(R_0 \cdots R_{N(n-1)} \cdots R_l \cdots R_{N(n)})}) \right| \geq \epsilon, \tag{4}$$

where we have adopted the lexicographic ordering for the monomials $\{X^i Y^j\}_{i+j \leq n}$, so that R_k stands for the kth column of the determinant (3) and $\widehat{R}_l = U$.

Then we can prove [12] the following theorem that describes the asymptotic behavior of the leading coefficients of the approximation in the mean of a piecewise smooth function:

Theorem 2.3 *Let ϵ be a positive real number and $\mathcal{S}$ an admissible stencil for degree n such that there exists an affine transformation $\mathcal{A}$ as in theorem 2.1 for which $\mathcal{A}(\mathcal{S}) \in \mathcal{P}_\epsilon^n$. Let (x_0, y_0) be any point of the set $K(\mathcal{S})$ and u be a real valued function defined on a open subset Ω of $\mathbb{R}^2$ containing $K(\mathcal{S})$. We assume that u is in C^{p-1}, $p < n$, on Ω and, except*

on a locally C^1 curve, admits a continuous and bounded p^{th} derivative with a jump $[D^p u]$, $|[D^p u]| > M_p > 0$. Then, the highest degree coefficients of the Taylor expansion of P_u satisfy

$$\sum_{i+j=n} |a_{ij}| \geq C(n,p,\epsilon) \frac{M_p}{h^{n-p}} \qquad (5)$$

where $C(n,p,\epsilon)$ is a constant independent of $\mathcal{S}$ and invariant by affine transformation.

2.4 Study of the linear problem to solve for the reconstruction

In this section, we study the numerical system one solves to get P_u from the data. We consider two kinds of expansions of P_u:

(i) The "natural" expansion: for any point $(x_0, y_0) \in \mathbb{R}^2$,

$$P_u = \sum_{i+j \leq n} a_{ij}(X - x_0)^i (Y - y_0)^j \qquad (6)$$

(ii) An expansion using "barycentric" coordinates that we now describe: let $\mathcal{S}^{(n)} = \{ C_1, C_2, C_3, \ldots, C_\Lambda$ be an admissible stencil. Hence, at least one subset of three elements of $\mathcal{S}^{(n)}$ is an admissible stencil for $n = 1$. We may assume that the set $\{C_1, C_2, C_3\}$ is admissible. We consider the three polynomials Λ_i of degree 1 defined by:

$$< \Lambda_i >_{C_j} = \delta_i^j, \quad 1 \leq i \leq 3, \quad 1 \leq j \leq 3. \qquad (7)$$

The symbol δ_i^j is the Kronecker symbol. Clearly, we have

$$\Lambda_1 + \Lambda_2 + \Lambda_3 = 1.$$

These polynomials are the barycentric coordinates of the triangle constructed on the gravity centers of C_1, C_2, and C_3. In order to get expansion 6, a strategy may be to look first for the expansion of the polynomial P_u in terms of power of Λ_2 and Λ_3:

$$P = \sum_{i+j \leq n} a_{ij} \Lambda_2^i \Lambda_3^j \qquad (8)$$

and then to get the Taylor expansion of P_u around the barycenter of C_1 from (8) (the theorems 2.1 and 2.3 give the behavior of the leading coefficients of P_u whatever the point chosen in the convex hull of $\mathcal{S}$).

In order to get the expansions (6) or (8), one has to solve linear $N(n) \times N(n)$ systems:

$$\mathcal{B}(a_{00} \ \cdots \ a_{0n})^T = (< u >_{C_{i_1}} \ \cdots \ < u >_{C_{i_{N(n)}}})^T \qquad (9)$$

where the matrix $\mathcal{B}$ is obtained by taking the average of $(X - x_0)^i (Y - y_0)^j$ for (6) and $\Lambda_2^i \Lambda_3^j$ for (8). Let us now study the properties of these linear systems.

8

2.4.1 Case of expansion (6)

A very easy consequence of the inequality (5) is that:

Proposition 2.4 *Let us assume that the conditions of theorem 2.3 holds, and let h be the supremum of the diameters of the spheres containing $K(\mathcal{S}^{(n)})$. Then the condition number of system (9) is at least $O(h^{-n})$ for h small enough.*

Proof: For the sake of simplicity we consider the following norm on $\mathbb{R}_n[X, Y]$: for $P = \sum_{i+j \leq n} a_{ij}(X - x_0)^i (Y - y_0)^j$, $\|P\| = \sum_{i+j \leq n} |a_{ij}|$. On $\mathbb{R}^{N(n)}$, we consider the L^1 norm. Let U be a set of data for the right hand side of (9), and consider the perturbation δU,

$$\delta U = (0 \cdots \epsilon \cdots)^T$$

where ϵ is at the l th position, $l \geq N(n - 1) + 1$. All the other entries of U are zero. If one considers the function u defined on $\bigcup \mathcal{C}_i$ by

$$x \in C_i, \quad u(x) = \delta U_i,$$

one can apply theorem 2.3. Hence, the perturbation δP has a norm satisfying

$$\|\delta P\| \geq \sum_{i+j=n} |\delta a_{ij}| \geq C \frac{\epsilon}{h^n}$$

since $\|\delta U\| = \epsilon$. This complete the proof. $\square$

This fact is well known for 1D Lagrange interpolation and has motivated the search for more efficient algorithms, such as the Newton algorithm. There exist algorithms that generalizes it [18, 19]. They involve numerous solutions of linear systems, so that we have preferred a more classical approach (see section 2.5), for which the coefficients of the linear systems are obtained from the "barycentric" coordinate expansion (8) as it is explained now.

2.4.2 Case of expansion (8)

In the case of expansion (8), we have the following result:

Proposition 2.5 *If property 2.2 holds for some $\epsilon > 0$, then the condition number of the system (9) for the expansion (8) is bounded above and below by constants independent of h, the supremum of the diameters of the circles containing $K(\mathcal{S}^{(n)})$.*

Proof: The proof is also based on that of theorem 2.3. As in proposition 2.4, the only thing that we have to do is to study the effect on the a_{ij}'s of a perturbation δU. We denote by P the polynomial whose averages are defined by δU. The proof can be achieved in two stages:

9

(i) Let B any invertible matrix. Consider the stencil

$$\widehat{\mathcal{S}^{(n)}} = \left\{ B[C_{i_j}] + x_0 \right\}_{1 \le j \le N(n)}$$

for any x_0. It is clear from the definition of the Λ_i's that $\widehat{\Lambda}_i(\widehat{x}) = \Lambda_i(x)$ if $\widehat{x} = Bx + x_0$. Hence, the sum $S(P)$ of the absolute values of the coefficients of P in the basis $\Lambda_2^i(x)\Lambda_3^j(x)$ is the same as that of the development of P in the basis $\widehat{\Lambda}_2^i(\widehat{x})\widehat{\Lambda}_3^j(\widehat{x})$. This is a homogeneity property.

(ii) Since the set of stencils defined by property (2.2) is compact, $S(P)$ is bounded below and above, independently of B, hence independently of h:

$$C_1 \ge F \ge C_2(\epsilon, n) > 0.$$

The constant $C_2(\epsilon, n)$ is larger than zero because $\delta U \ne 0$

This achieves the proof $\square$

2.5 The explicit calculation of the reconstruction

From the previous results, the evaluation of the coefficients a_{ij} in (6) is done through those of (8) and hierarchally. For the sake of simplicity, we assume that for any $p \le n$, the set $\mathcal{S}^{(p)}$ of the $N(p)$ first elements of $\mathcal{S}^{(n)}$ is an admissible set for order p. This can be achieved with a suitable numbering of the elements of $\mathcal{S}^{(n)}$. The idea is that instead of looking directly for the coefficients of $P^{(n)}$, to get first those of all of the $P^{(k)}$'s, the reconstruction over $\mathcal{S}^{(k)}$, for $1 \le k \le n$. Then to construct those of $P^{(n)}$. In the ENO algorithm described in section 2.6, this involves *no* extra cost and simplifies the evaluation of the a_{ij}'s. This also has the advantage of reducing the size of the linear systems and also of improving their condition numbers.

Assume that $P^{(1)}, \ldots, P^{(p)}$ are known. We first compute the coefficients of $P^{(p+1)} - P^{(p)}$,

$$P^{(p+1)} - P^{(p)} = \sum_{i+j \le p+1} a'_{ij} \Lambda_2^i \Lambda_3^j$$

by solving the linear system

$$A_{p+1} \begin{pmatrix} \underline{a_1} \\ \underline{a_2} \end{pmatrix} = \begin{pmatrix} A_p & B_{p\ p+1} \\ C_{p\ p+1} & D_{p\ p+1} \end{pmatrix} \begin{pmatrix} \underline{a_1} \\ \underline{a_2} \end{pmatrix} = \begin{pmatrix} \underline{u_1} \\ \underline{u_2} \end{pmatrix} \tag{10}$$

In equation (10), $\underline{a_1}$ (respectively $\underline{a_2}$) stands for the coefficients $\{a_{ij}\}_{i+j \le p}$ (resp. $\{a_{ij}\}_{i+j=p+1}$). The block matrices A_p, $B_{p\ p+1}$, $C_{p\ p+1}$ and $D_{p\ p+1}$ are defined according to this decomposition. In particular, we notice from the hypothesis that A_p is invertible.

From the conservation property, we get $\underline{u_1} = 0$, so that the system (10) can be split:

$$\underline{a_1} = -A_p^{-1} B_{p\ p+1} \underline{a_2}$$

$$\left[-C_{p\ p+1} A_p^{-1} B_{p\ p+1} + D_{p\ p+1} \right] \underline{a_2} = \underline{u_2}$$

(11)

Since $\mathcal{S}^{(p+1)}$ is admissible, $E_p = \left[-C_{p\ p+1} A_p^{-1} B_{p\ p+1} + D_{p\ p+1} \right]$ is also invertible, so that one can get $\underline{a_2}$, then $\underline{a_1}$, and finally the coefficients of $P^{(p+1)}$.

Simple manipulations show that

$$A_{p+1}^{-1} = \begin{pmatrix} A_p^{-1} B_{p\ p+1} E_p^{-1} C_{p\ p+1} A_p^{-1} + A_p^{-1} & -A_p^{-1} B_{p\ p+1} E_p^{-1} \\ -E_p^{-1} C_{p\ p+1} A_p^{-1} & E_p^{-1} \end{pmatrix}$$

so that one can quite easily go to the next step. In our case, since the total degree of the reconstruction is less or equal to 4, at most two stages of this method are needed.

Finally, one must notice that the condition number of this method is always better that that of the original one because it depends only on part of the original system.

2.6 The E.N.O. reconstruction

In [12], we have found that only a few stencils were indeed necessary to achieve an essentially non-oscillatory reconstruction of a piecewise smooth function. This set has to be as isotropic as possible. Moreover, the ENO reconstruction was found to achieve the expected order of accuracy for smooth functions, even on very irregular meshes. In what follows a_{ij} always stands for any of the coefficients of the reconstruction P in the natural basis, $\{(X - x_0)^i (Y - y_0)^j\}$. Let us describe our procedure up to fourth order:

(i) Let us start from a given cell, C_0 assigned to a point of $\mathcal{M}$, say (x_0, y_0).

(ii) Consider all the triangles having (x_0, y_0) as a vertex, and choose the one, say T_{min}, that minimize

$$\sum_{i+j=1} |a_{ij}|.$$

Here, $\mathcal{S}^{(1)}$ is the set of control volumes corresponding to the vertices of T_{min}, (see Figure 3-a). For a regular unstructured mesh, there are about six possible triangles.

(iii) Consider T_{min}. For any of its three edges, consider the three triangles, T_1, T_2, T_3 as in Figure 3-a. There are three possible configurations. We choose the one that minimizes the sum

$$\sum_{i+j=2} |a_{ij}|.$$

11

(iv) Consider, as in Figure 3-b, the configuration for third order. It is obtained as follows: for a stencil $\mathcal{S}^{(2)}$ made of the control volumes associated with the vertices of $\{T_{min}, T_1, T_2, T_3\}$, one may consider its "edges" made of the external sides of $\{T_2, T_3\}$, $\{T_2, T_{min}\}$, $\{T_{min}, T_3\}$. Consider one of them, say $\{T_2, T_3\}$, and the vertices α, β and γ. Since the triangulation is conformal, there exist a triangle $T_4 \neq T_2$ on the other side of $[\alpha, \beta]$. Similarly, T_5 for $[\beta, \gamma]$. Then one can construct T_6, T_7, T_8 and T_9, analogously. The stencils for fourth order reconstruction are the union of $\mathcal{S}^{(2)}$ and the control volumes associated with the additional vertices of either $\{T_4, T_5, T_6, T_7\}$ or $\{T_4, T_5, T_9, T_8\}$ or $\{T_4, T_5, T_7, T_8\}$. For a stencil $\mathcal{S}^{(2)}$, there are at most 12 stencils for fourth order reconstruction.

The situations seem to be become more and more complicated as the degree increases. Nevertheless, there is a very easy way to simplify it, so that at each level only three new stencils for the $n + 1^{th}$ order have to be considered over those of a nth order one, just as from second order to third order. Assuming a mesh $\mathcal{M}$, we want to derive a $k + 1^{th}$ order reconstruction method. The idea is to work with the control volumes defined for a mesh $\mathcal{M}'$, the points and the triangulation of which are constructed from those of $\mathcal{M}$ by adding, for each triangle of $\mathcal{M}$, the points and the triangles associated with the P_k Lagrange interpolation [20].

3 A class of high order numerical scheme for compressible flow simulations

3.1 The Euler equations

Let us quickly recall elementary things about the Euler equation of a calorically perfect gas:

$$\frac{\partial W}{\partial t} + \frac{\partial F(W)}{\partial x} + \frac{\partial G(W)}{\partial y} = 0 \tag{12}$$

As usual, in equation (12), W stands for the vector of conserved quantities and F (respectively G) is the flux in the x direction (resp. y direction):

$$W = \begin{pmatrix} \rho \\ \rho\, u \\ \rho\, v \\ E \end{pmatrix} \quad F(W) = \begin{pmatrix} \rho\, u \\ \rho\, u^2 + p \\ \rho\, uv \\ u(E + p) \end{pmatrix} \quad G(W) = \begin{pmatrix} \rho\, v \\ \rho\, uv \\ \rho\, v^2 + p \\ v(E + p) \end{pmatrix} \tag{13}$$

with initial and boundary conditions. In equation (13), ρ is the density, u, v are the components of the velocity, E is the total energy, and p the pressure, related to the conserved

quantities by the equation of state:

$$p = (\gamma - 1)\left(E - \frac{1}{2}\rho(u^2 + v^2)\right) \tag{14}$$

The ratio of specific heats, γ, is kept constant.

It is well known that the system defined by equations (12), (13) and (14) is hyperbolic: for any vector $\vec{n} = (n_x, n_y)$, the matrix

$$A_{\vec{n}} = n_x \frac{\partial F}{\partial W} + n_y \frac{\partial G}{\partial W} \tag{15}$$

is diagonalizable and has real eigenvalues and eigenvectors. Let us describe now the construction of a kth order scheme.

3.2   Finite volume formulation

We consider a mesh $\mathcal{M}$ and the control volumes as in figure 2. The semi discrete finite volume formulation of (12) is:

$$\frac{\partial}{\partial t}\overline{W}_i(t) = -\frac{1}{area(\mathcal{C}_i)}\int_{\partial \mathcal{C}_i} \mathcal{F}_{\vec{n}}[W(x,t)]dl = \mathcal{L}_i(t) \tag{16}$$

Here $W(t)$ is the (spatial) mean value of $W(x,t)$ at time t over $\mathcal{C}_i$, $\vec{n} = (n_x, n_y)$ is the outward unit normal to $\partial \mathcal{C}_i$, and $\mathcal{F}_{\vec{n}} = n_x F + n_y G$. We first describe the spatial approximation of (16), then the temporal discretization of the resulting set of ordinary differential equations. Finally, we detail the boundary conditions.

3.2.1   Spatial discretization

For the sake of simplicity we define the integer number p such that either $k = 2p$ or $k = 2p+1$. The first step is to discretize $\mathcal{L}_i(t)$ up to k^{th} order. First, we can rewrite $area(\mathcal{C}_i)\mathcal{L}_i(t)$ as

$$\int_{\partial \mathcal{C}_i} F_{\vec{n}}[W(x,t)]dl = \sum_{\Gamma_s}\int_{\Gamma_s} F_{\vec{n}}[W(x,t)]dl \tag{17}$$

where, as in figure 2, the set Γ_s's is that of the linear edges of $\mathcal{C}_i$. On each Γ_s, $\vec{n}$ is constant. We consider on any Γ_s the p Gaussian points $\{G_l\}_{1 \le l \le p}$ associated to the Gaussian formula of order $2p + 1$. The integral $\int_{\Gamma_s} F_{\vec{n}}[W(x,t)]dl$ is approximated by

$$\sum_{l=1}^{p} \omega_l \mathcal{G}_{\vec{n},l}(t) \tag{18}$$

where term $\mathcal{G}_{\vec{n},l}(t)$ is defined now. Set $\mathcal{C}_j$ is the other control volume of which Γ_s is a part of the boundary. In $\mathcal{C}_i$ and $\mathcal{C}_j$, one computes the ENO reconstructions at time t of W,

$R_i[W(\,.\,,t),k]$ and $R_j[W(\,.\,,t),k]$, up to order k. The ENO reconstruction of section 2 is applied to the physical variables, then one deduce the conserved ones. From that, we set, in equation (18):

$$\mathcal{G}_{\vec{n},l}(t) = \mathcal{F}_{\vec{n}}^{\text{Riemann}}\left\{ R_i[W(\,.\,,t),k](G_l), R_j[W(\,.\,,t),k](G_l) \right\}. \tag{19}$$

In equation (19), $\mathcal{F}_{\vec{n}}^{\text{Riemann}}$ may be any of the available Riemann solvers. In all the example below, we have chosen Roe's Riemann solver with the Harten-Hyman entropy correction.

3.2.2 Temporal discretization

The equations (16), (17), (18) and (19) define a finite set of ordinary differential equations that we write as:

$$\frac{\partial}{\partial t}\overline{W}_i(t) = \tilde{\mathcal{L}}_i(t) \tag{20}$$

In (20), $\tilde{\mathcal{L}}_i(t)$ is the discrete version of $\mathcal{L}_i(t)$. This equation is discretized by the kth order version of the Runge-Kutta scheme of Shu [9]:

$$\begin{cases} W_i^{(l)} = \sum_{m=0}^{l-1}[\alpha_{lm}W_i^{(m)} + \beta_{lm}\tilde{\mathcal{L}}_i^{(m)}], & l = 1,2,\cdots,p, \quad \tilde{\mathcal{L}}_i^{(m)} = \tilde{\mathcal{L}}_i(W_i^{(m)}) \\ \\ W_i^{(0)} = W_i^n, \qquad\qquad W_i^{(p)} = W_i^{n+1}. \end{cases} \tag{21}$$

The order of accuracy, as well as its TVD properties, is achieved by adequate sets of coefficients α_{lm}, β_{lm}, and p (see [9] for details).

3.2.3 Boundary conditions

Let Γ be the boundary of the computational domain and $\vec{n}$ be the outward normal unit on Γ. We assume that Γ is divided into two parts, $\Gamma = \Gamma_0 \cap \Gamma_\infty$, on which different boundary conditions will be used. Here, Γ_0 represents a solid wall, while Γ_∞ represents the far-field (inflow or outflow).

We do not treat a boundary conditions by forcing the value of a variable to a prescribed boundary value, but consider instead the integral formulation (16) and apply boundary condition by modifying the flux integrals on $\partial \mathcal{C}_i$ for those cells with $\Gamma \cap \partial \mathcal{C}_i \neq \emptyset$.

For example, for a vertex i located on Γ_0, we do not impose the slip condition $\vec{U}\cdot\vec{n} = 0$ but take this condition into account in the evaluation of the convective flux

$$\int_{\Gamma_0 \cap \partial \mathcal{C}_i} Fn_x + Gn_y = \begin{bmatrix} 0 \\ \int_{\Gamma_0 \cap \partial \mathcal{C}_i} pn_x \\ \int_{\Gamma_0 \cap \partial \mathcal{C}_i} pn_y \\ 0 \end{bmatrix}.$$

The pressure integrals are computed as:

$$\int_{\Gamma_0 \bigcap \partial C_i} pn_x \simeq p_i \int_{\Gamma_0 \bigcap \partial C_i} n_x, \qquad \int_{\Gamma_0 \bigcap \partial C_i} pn_y \simeq p_i \int_{\Gamma_0 \bigcap \partial C_i} n_x.$$

For a vertex located on Γ_∞, we again use an approximate Riemann solver. We define a far field state W_∞, $\vec{n}_i = \int_{\Gamma_\infty \bigcap \partial C_i} \vec{n}$ and set, in agreement with what has been done in the interior of the computational domain,

$$\int_{\Gamma_\infty \bigcap \partial C_i} Fn_x + Gn_y = \Phi(W_i, W_\infty, \vec{n}_i). \qquad (22)$$

In equation (22), Φ is a numerical flux function. For simplicity, we have chosen a modified Steger-Warming flux instead of the Roe flux,

$$\Phi(W_i, W_\infty, \vec{n}) = A_{\vec{n}}^+ W_i + A_{\vec{n}}^- W_\infty.$$

The matrices $A_{\vec{n}}^+$ and $A_{\vec{n}}^-$ are the positive and negative parts of the matrix $A_{\vec{n}}$ defined in (15) and evaluated for $W = W_i$.

In all the examples we have treated below, the boundaries were either fully subsonic or fully supersonic, so that the procedure was really simple, contrary to what would have appeared in a mixed type boundary condition.

Finally, we have reduced the order of accuracy of the reconstruction for cells that are too near to the boundary. For them, a proper calculation of the ENO stencil may be impossible because the set of possible stencils is biased in one direction due to the boundary. For the third order scheme, these cells are those related to a mesh point that belongs to a triangle having at least one point on the boundary. For the fourth order scheme, they are those belonging to a triangle which shares a vertex with a cell for which a reduction of order must be done for third order.

3.3 Positivity of the density and the pressure

As pointed out by Harten et. al. [22], in some situation and for a very few cells, the ENO reconstruction of the density and pressure may lead to negative values. For these cells, and these cells only, following [22], we reduce the order of accuracy with the following inductive method (w is either the density or the pressure, w_i is its average on C_i). Consider, in C_i, the reconstruction

$$R[w,n](X,Y) = \sum_{l=0}^{n} \sum_{p+q=l} a_{pq}(X - x_g)^p (Y - y_g)^q,$$

If $\sum_{l=2}^{n} \sum_{p+q=l} |a_{pq}||(x - x_g)^p (y - y_g)^q| \geq \alpha |w_i|$ at a Gaussian point (x, y), then the reconstruction, for that point, is set to $R[w, n-1](x, y)$. Then, we repeat the test if necessary. Usually, the parameter α is set to 0.95.

15

In all the simulations we have done, the tests were positive for a very small set of cells and a zeroth order reconstruction was never used. They were never positive for the second order scheme. The number of points causing difficulty is problem dependent. For example, only three points caused occasional problems for the facing step problem with a 5000 node mesh. These points were all located in the front shock.

4   Numerical tests

All the example we propose now have been computed with the second and third ENO schemes. The ratio of specific heats, γ is always set to 1.4.

4.1   A linear advection problem

In order to test the precision of these scheme, we have computed the advection of sine wave on a sequence of totally unstructured meshes with an increasing number of points. The convection velocity was parallel to the x axis but since the meshes was totally unstructured, this is not a privileged direction. Figure 4 shows, in the abscissa, the logarithm of the maximum radius of the circumscribed circles of the triangles of the meshes, and in the ordinate, the logarithm of the maximum absolute value of the difference between the computed values. The exact solution is also indicated. The slopes -2 and -3 are indicated, so that one can see that the expected order of accuracy is indeed achieved. Figure 5 shows, for the medium mesh, a cross section of the computed solution for the second and third order scheme. The exact cross section is also indicated. One can see that the main differences lies at the extrema of the sine, as expected.

4.2   A Shock tube problem

We have set up a two dimensional shock tube problem in the square $[0,1] \times [0,1]$. Its boundary are solid. The initial conditions are:

$$\text{for} x \le 0.5 \text{ and } |y - 0.5| \le 0.25, \quad \begin{cases} \rho = 1.0 \\ u = v = 0.0 \\ p = 1.0 \end{cases}$$

$$\text{else} \quad \begin{cases} \rho = 0.125 \\ u = v = 0.0 \\ p = 0.1 \end{cases}$$

The mesh is completely unstructured with 2127 nodes and 4088 triangles. The velocity field obtained by the third order scheme at time $t = 0.9$ is displayed in Figure 6. The differences

between both results are more clearly visible in the near stagnation zone. In order to better represent that area, we have removed from the velocity field all the points for which the sum of the absolute values of the two components is larger than 0.15. The result is shown in Figures 7 (second order) and 8 (third order). One can clearly observe that the number of small structures of the flow is much more important in Fig. 8 than in Fig. 7. The shocks in the upper and lower part of the pictures are also resolved differently. Their location is also different, though this can be seen only by superimposing the pictures.

One should also mention that this test is not particularly easy for our method. After a short time, the shock reflects from the wall. The reflected shock interacts with the others structures of the flow, leading to interactions between the various kind of discontinuities and with the smooth parts of the flow. The multiple regions, as shown on our figures, with different kind of discontinuities (contact and shock) are resolved by our method without any special tricks.

4.3   A Mach 3 wind tunnel with a step

We have run this test case, documented in [23], for the second order and third order ENO schemes on a 5140 node, 9958 triangle mesh. This discretization corresponds to the medium mesh used in [23]. A portion of it is displayed in Figure 9. It is totally unstructured. The conditions of the problem are the following: a uniform Mach 3 flow is set in a channel. At the initial time, a step of relative height 0.2 is installed in the channel. The channel length is 3 and the step is located at 0.6. This situation creates a shock that reflects on the upper part of the channel then evolves to a lambda shock as time increases. It interacts with the upper part of the step. A weak shock is also created by the expansion wave at the corner. This shock interacts with the reflected one creating a slip line. The location of this slip line is highly dependent on the boundary conditions set at the corner.

Here, no special treatment is done, contrary to what was advocated in [23], so that the quality of the second reflected shock is poor. We only want to verify the effect of the increasing order of accuracy on the solution, so that we will only look at the first reflected shock. The solutions of Figure 10 (second order ENO) and Figure 11 (third order ENO) are shown. A clear improvement on the thickness of that reflected shock can be seen from the horizontal cross section of the density at $y = 0.5$, Figure 12. The slip line coming from the lambda shock is also more visible in Figure 11 than in Figure 10 as well as the weak shock near the corner.

17

4.4 Reflection of a shock on a wedge

This problem is also well documented in the literature. In order to achieve a correct solution, one has either to use very fine meshes or adapted meshes (see [5] for example). We have chosen a case where the planar shock enters from the left in a quiescent fluid. Its Mach number is $M_S = 5.5$ and is defined for the flow values in the quiescent fluid where the density is set to 1.4 and the pressure to 1. One expects a double Mach reflection.

The mesh has only 8569 points and 16806 triangles. A part of it is shown in Figure 13. The density contours of the two calculations are displayed in Figures 14 (second order) and Figure 15 (third order). A very clear improvement of the slip line coming from the Mach stem can be observed. The second triple point can also been observed in Figure 15, though it is of poor quality because of the insufficient resolution of the present mesh. It is, however, totally obscured in Figure 14. Generally speaking, all the discontinuities are better resolved by the third order scheme.

5 Conclusions

A third order ENO scheme has been derived for triangular unstructured meshes; this demonstrates the possibility of deriving ENO schemes for unstructured meshes. We indicate how to build higher order ENO schemes and give some comments on the numerical stability of the reconstruction step.

Our new scheme has been tested on a set of well known test cases and compared to a second order scheme. In all cases, the results are clearly improved. Our results also demonstrate the scheme's robustness. The cost of the scheme is four times that of the second order scheme (on a Cray YMP) even though the new code is far from being optimized. In particular, no optimization has been done in the ENO reconstruction procedure, the most expensive routine, so that the factor of four is clearly a poor upper bound on the cost ratio.

In the near future, we will derive the fourth order version of this class of schemes. The two schemes will then be coupled with a dynamic adaptation procedure [3] to improve their efficiency.

References

[1] H.C. Yee. *Upwind and Symmetric Shock-Capturing Schemes.* Technical Report TM–89464, NASA, May 1987.

[2] L. Fezoui, B. Stoufflet. A Class of Implicit Upwind Schemes for Euler Simulations with Unstructured Meshes. *Journal of Computational Physics*, 84(1) pp : 174–206, September 1989.

[3] N. Maman and B. Larrouturou. Dynamical mesh adaptation for two-dimensional reactive flow simulation, *Numerical Grid Generation in Computational Fluid Dynamics and Related Field*, S.-Arcilla, A. and Häuser, J. and Eiseman, P. R. and Thompson, J. F. Eds, Elsevier Science Publishers B. V., pp. 13–26, 1991

[4] B. Palmerio & A. Dervieux. The Capture of Viscous Layers by Non-Structured Mesh Deformation 13 th IMACS World Congress on Computation and Applied Mathematics, July 22, 26 1991, Dublin Ireland, To appear.

[5] J. J. Quirk. An Alternative to Unstructured Grids for Computing Gas Dynamic Flows around Arbitrarily Complex Two-Dimensional Bodies. Icase Report 92–7, February 1992.

[6] A. Harten & S. Osher. Uniformly High-Order Accurate Nonoscillatory Schemes-I, *SIAM Journal of Numerical Analysis*, Vol. 24, No 2, April 1987, pp. 279–309.

[7] A. Harten, S. Osher, B. Engquist & S. R. Chakravarthy. Some Results on Uniformly High-Order Accurate Essentially Nonoscillatory Schemes, Applied Numerical Analysis 2 (1986), pp. 347–377, Elsevier Science Publishers B.V (North Holland).

[8] A. Harten, B. Engquist, S. Osher & S. R. Chakravarthy. Uniformly High Order Accurate Essentially Non-Oscillatory Schemes III, *Journal of Computational Physics*, Vol 71, pp. 231–303. (1987).

[9] C.W. Shu & S. Osher. Efficient Implementation of Essentially Non-Oscillatory Shock-Capturing Schemes, *Journal of Computational Physics*, Vol 77, pp.439–471 (1988).

[10] A. Harten. ENO Schemes with Subcell Resolution, *Journal of Computational Physics*, Vol 83, pp.148–184 (1989).

[11] J. Casper & H.L. Atkins. A Finite-Volume Application of High Order ENO Schemes for Two-Dimensional Hyperbolic Systems, Submitted to the *Journal of Computational Physics*.

[12] R. Abgrall. Design of an Essentially Non-Oscillatory Reconstruction procedure on Finite-Elements type meshes, Icase report 91–84 (December 1991), in revised form INRIA Report No 1592 (January 1992), submitted to Math. of Comp.

[13] R. Abgrall. An Essentially Non Oscillatory Scheme on Unstructured Meshes, Proceedings of the Second International Conference on High Order and Spectral Methods, June 22-26, 1992. To appear as a special issue of *Computer Methods in Applied Mechanics and Engineering*, Elsevier, 1992

[14] A. Harten & S.R. Chakravarthy. Multi-Dimensional ENO Schemes for General Geometries, Icase Report No 91-76, September 1991, submitted to the Journal of Computational Physics.

[15] P. Vankeirsblick & H. Deconinck. Higher Order Upwind Finite Volume Schemes with ENO-properties for General Unstructured Meshes, Paper No 7, AGARD R–787, May 1992, unpublished.

[16] T. J. Barth & P.O. Frederickson. High Order Solution of the Euler Equations on Unstructured Grids using Quadratic reconstruction, Presented at AIAA, 28th Aerospace Sciences Meeting, January 8-11, 1990, Reno, Nevada.

[17] K.C. Chung & T. H. Yao. On Lattrices Admitting Unique Lagrange Interpolations, SIAM Journal of Numerical Analysis, Vol 14, No 4, September 1977, pp. 735–743.

[18] G. Muhlbach. The General Recurrence Relation for Divided Differences and the General Newton-Interpolation-Algorithm with Applications to Trigonometric Interpolation. Numerische Mathematik, Vol 32, pp. 393-408, 1979.

[19] G. Muhlbach. The General Neville-Aitken-Algorithm and Some Applications. Numerische Mathematik, Vol 31, pp. 97–110, 1978.

[20] G. Strang & G. J. Fix. An analysis of the finite element method. Prentice-Hall INC.,Englewood Cliffs, N.J., 1973

[21] P.G. Ciarlet & P. A. Raviart. General Lagrange and Hermite interpolation in $\mathbb{R}^n$ with application to Finite Element Methods. *Archive for Rational Mechanics and Analysis*, Vol 42, 1972, pp. 177–199.

[22] A. Harten, B. Engquist, S. Osher & S.K. Chakravarthy. Uniformly High Order Accurate Essentially Non-Oscillatory Schemes III, ICASE Report 86-22, April 1986.

[23] P. Woodward & Colella, The Numerical Simulation of Two-Dimensional Fluid Flow with Strong Shocks, *Journal of Computational Physics*, Vol 54, pp. 115–173, 1984
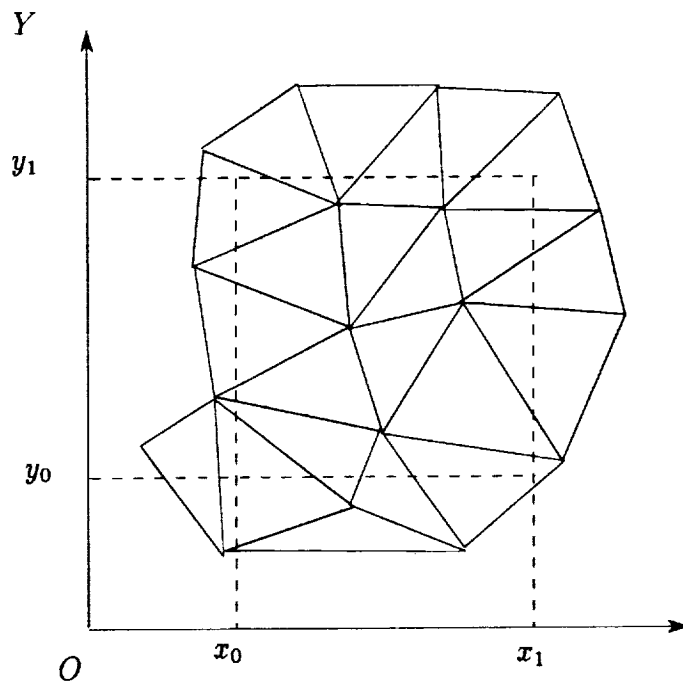
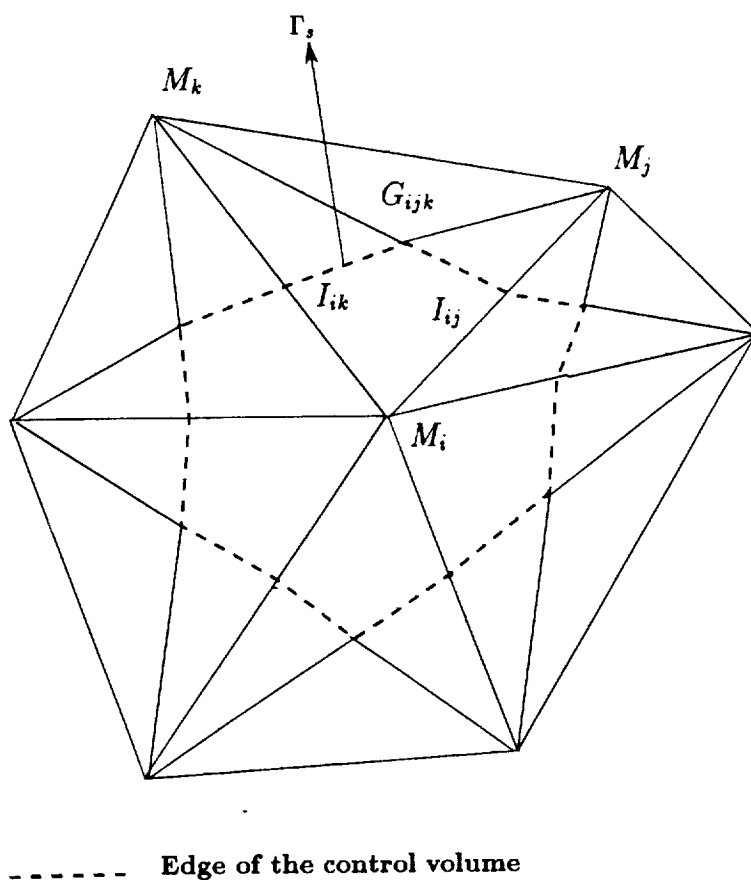Figure 1: Covering of the rectangle $[x_0, x_1] \times [y_0, y_1]$ by triangular control volumes
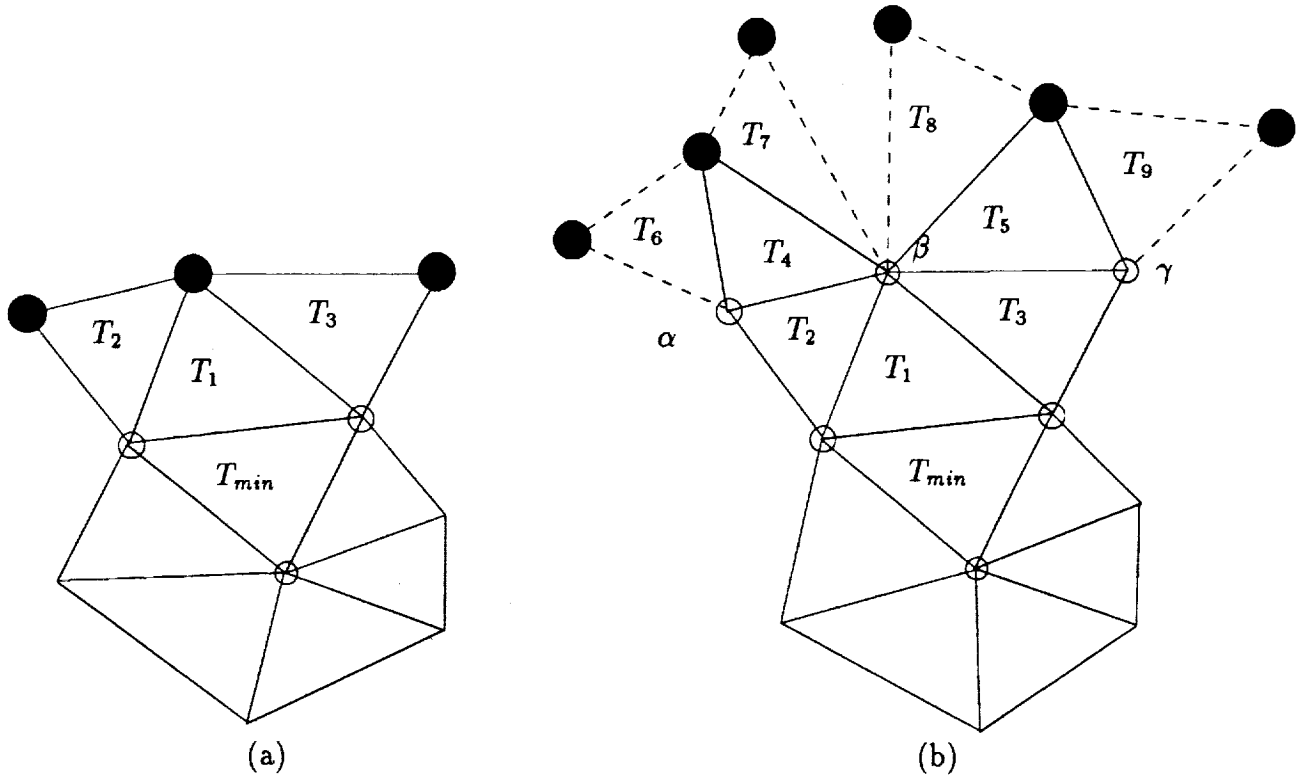
- - - - - - **Edge of the control volume**

Figure 2: Element of the dual mesh

Figure 3: Stencils for third and fourth order reconstruction
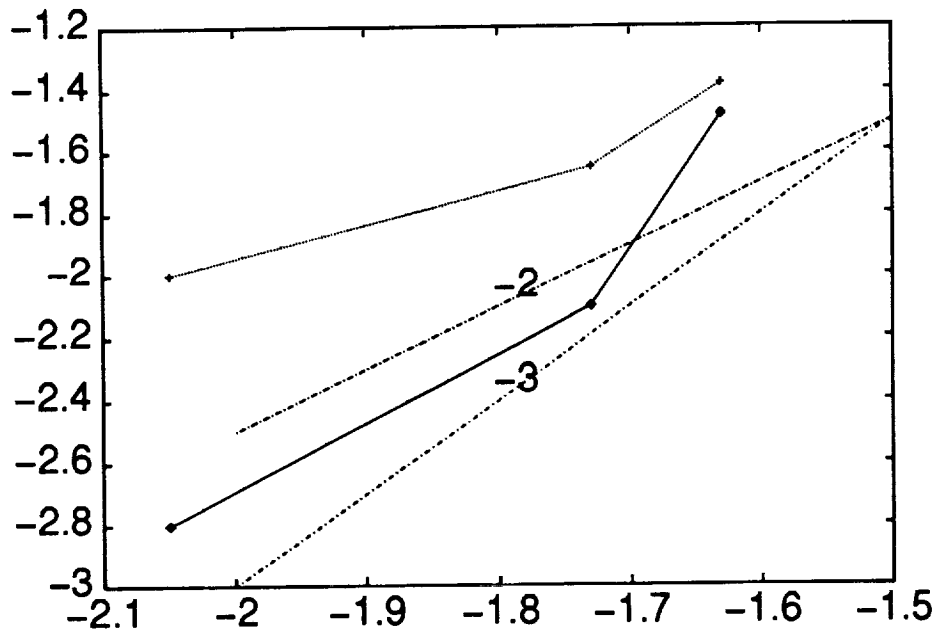
Figure 4: Representation of the logarithm of the L_∞ error in term of the logarithm of the maximum radius of the circumcircles.
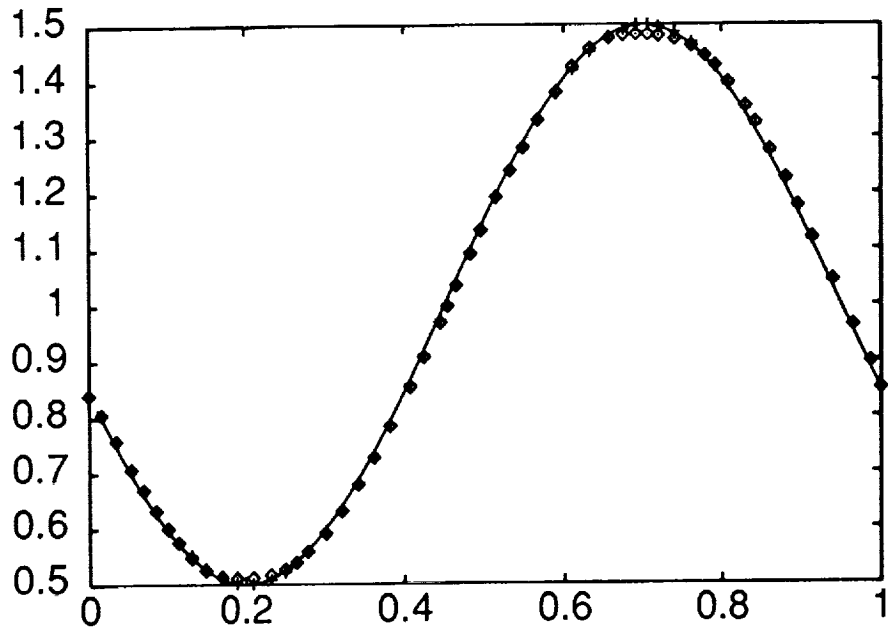
Figure 5: Advection of a sine wave, $\diamond$: second order, $+$: third order, plain line : exact
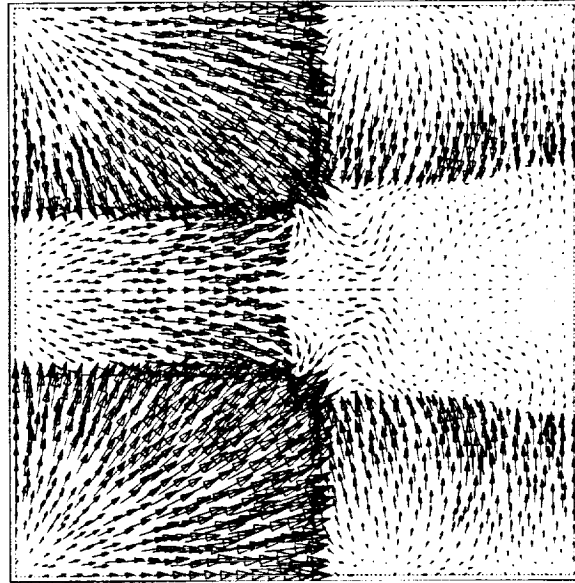
Figure 6: Shock tube : velocity field at time $t = 0.9$

27
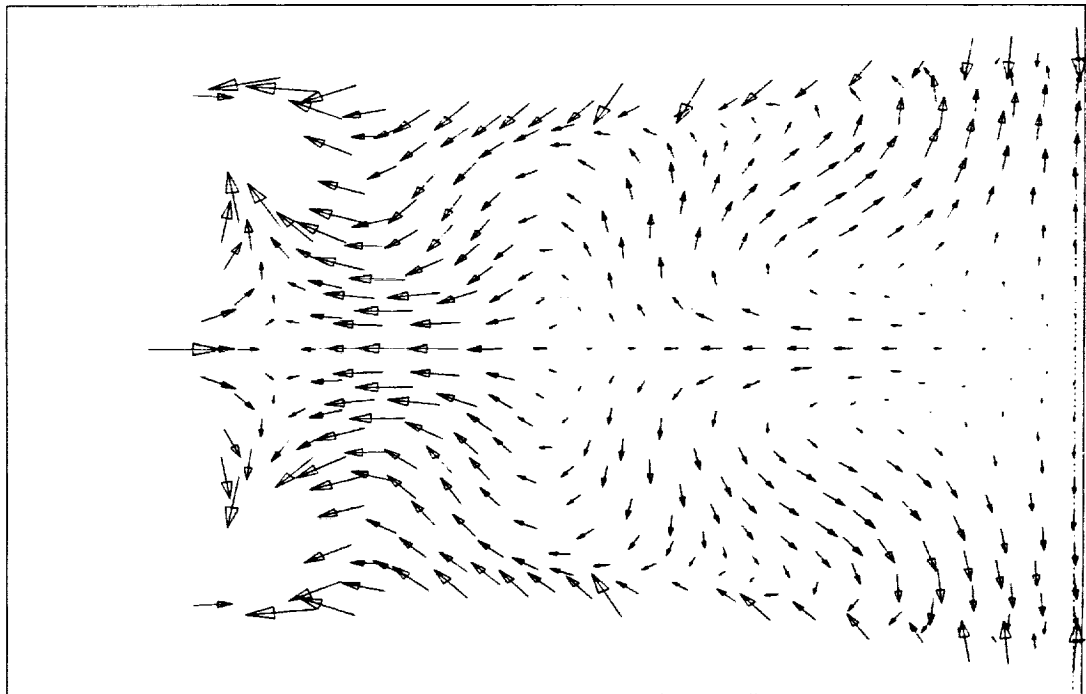
Figure 7: Zoom of the velocity field in $[0.5, 1] \times [0.25, 0.75]$. Second order solution
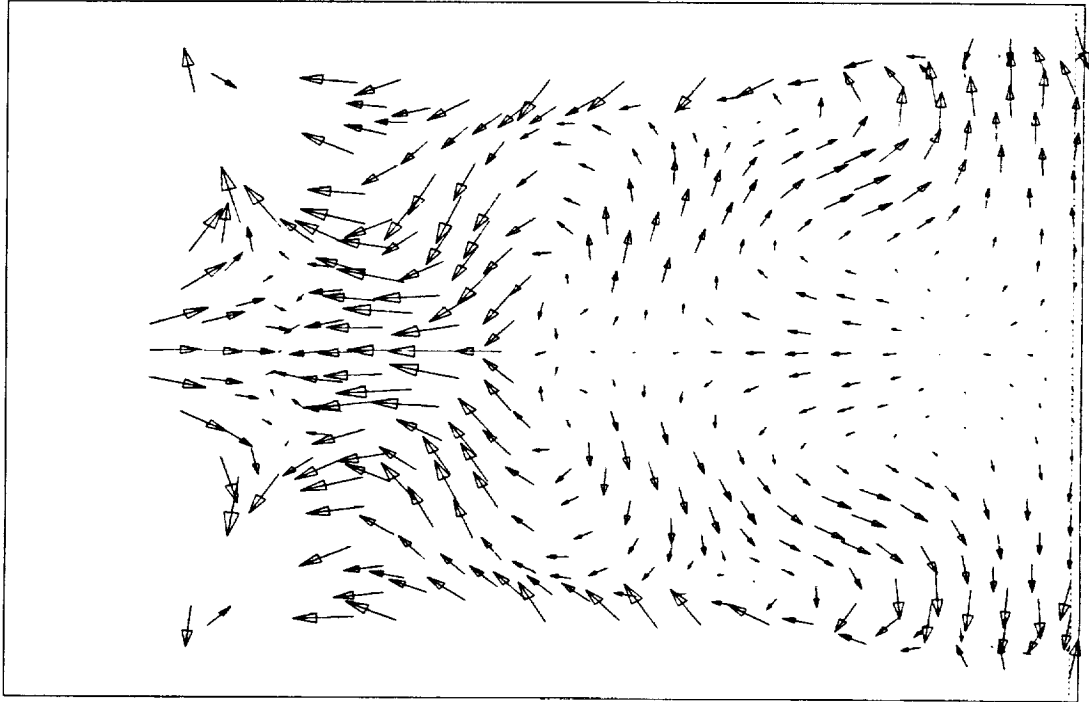
Figure 8: Zoom of the velocity field in $[0.5, 1] \times [0.25, 0.75]$. Third order solution
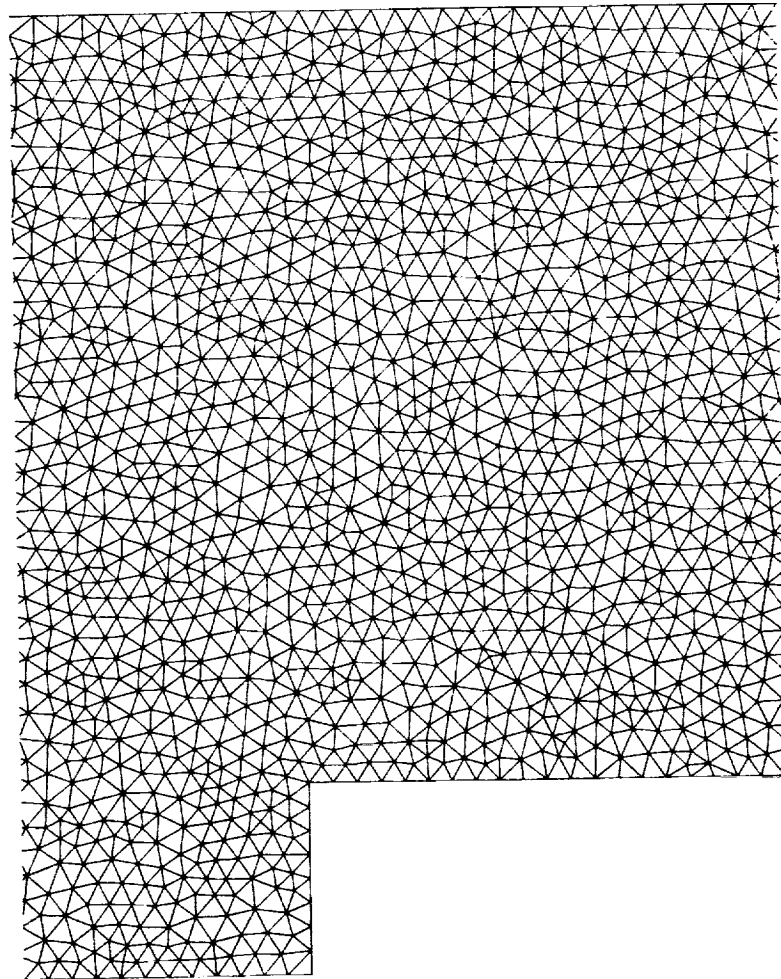
Figure 9: Portion of the mesh used for the step case
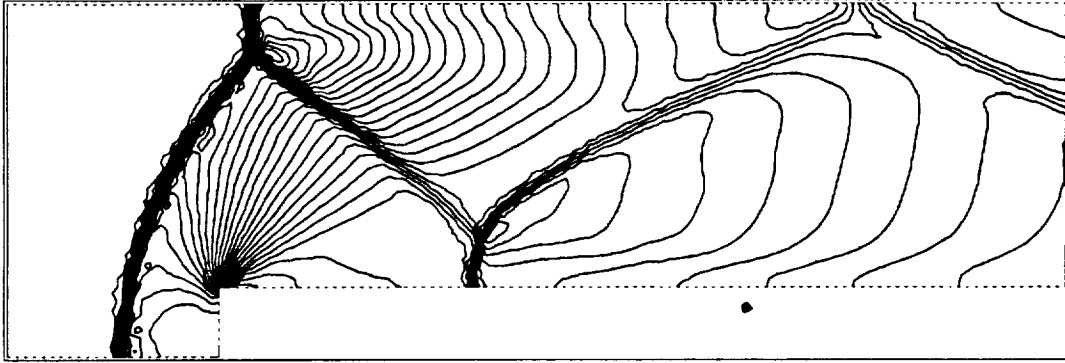
Figure 10: Density contours for the second order ENO solution, t=4, min=0.329, max=4.64. Density contours from 0.287 to 4.584, $\Delta\rho = 0.14$
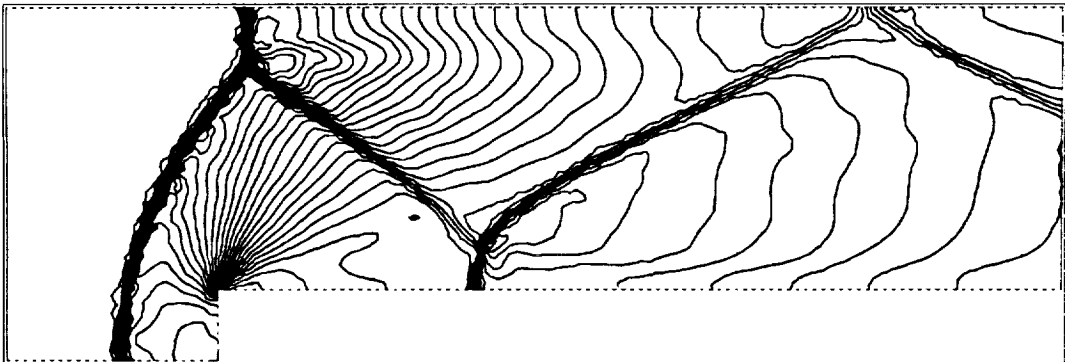

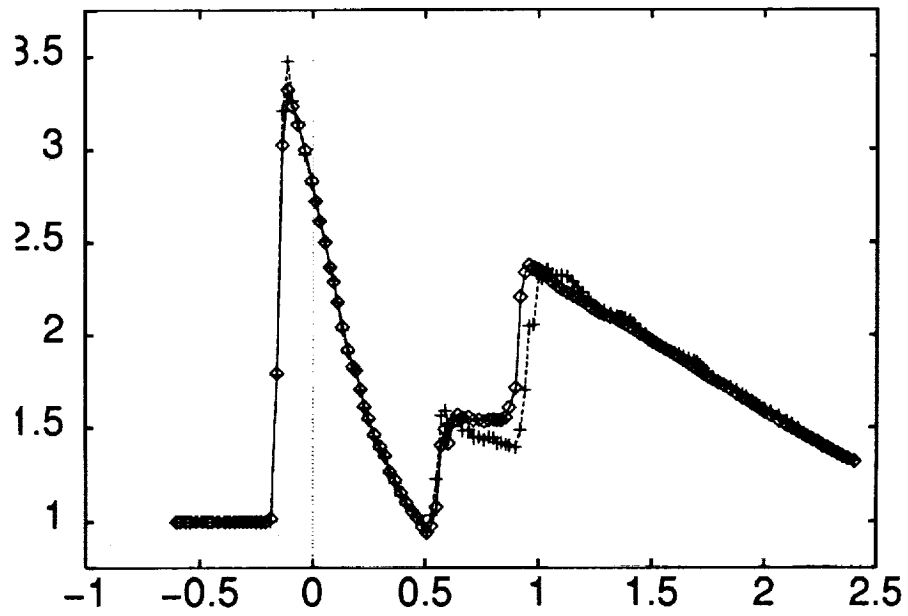Figure 11: Density contours for the third order ENO solution, t=4, min=0.287, max=4.584, $\Delta\rho = 0.14$

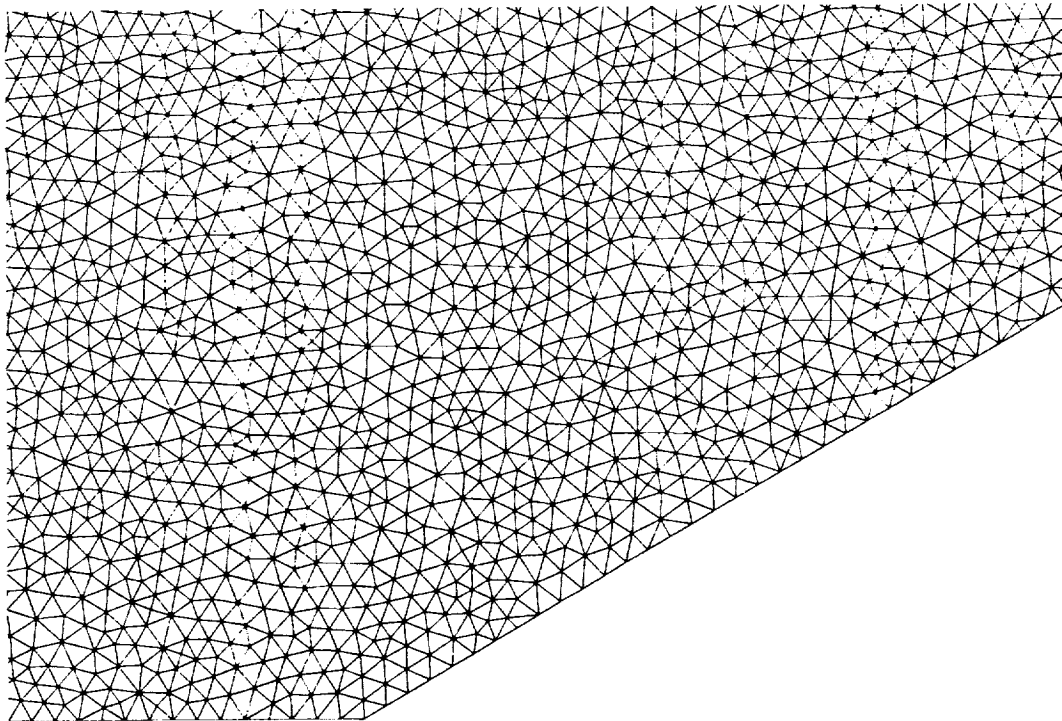Figure 12: Cross-section of the density, $y = 0.5$ ◇ : second order, + : third order

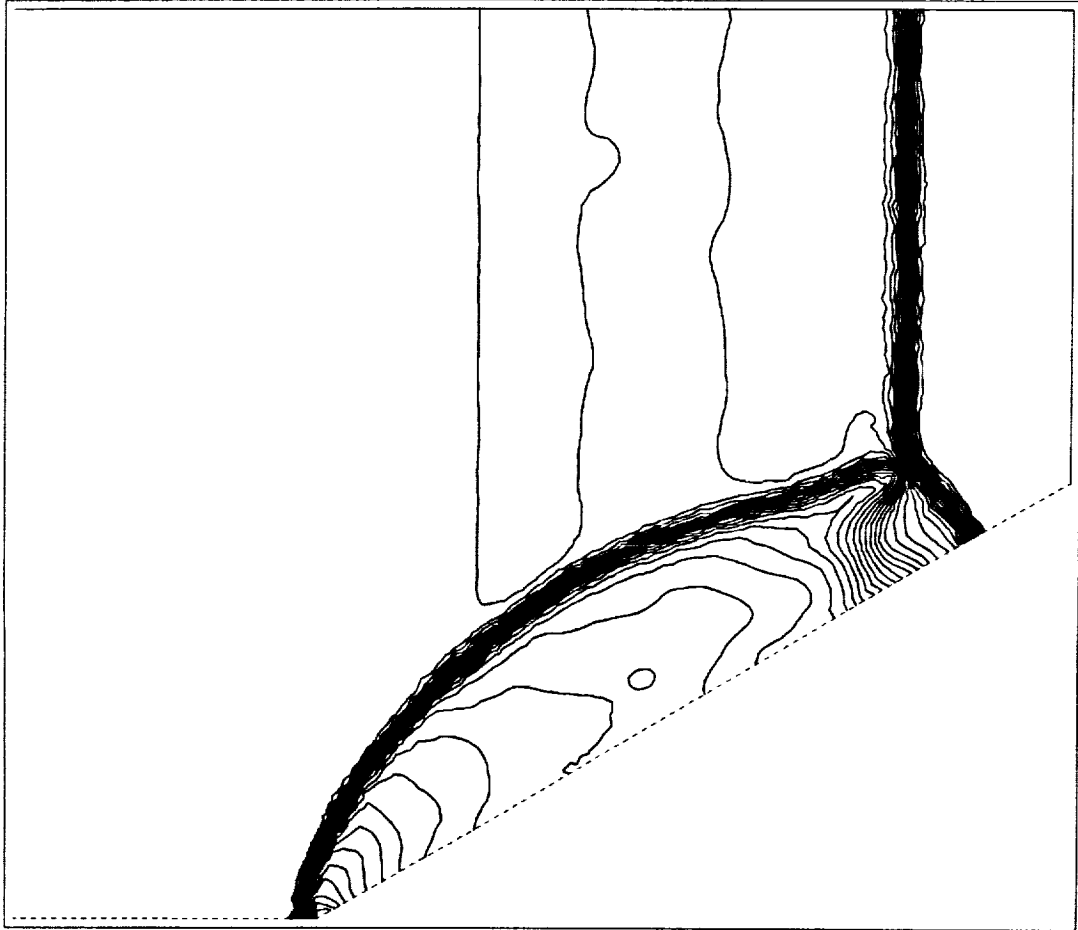Figure 13: Portion of the mesh used for the Mach reflection problem

Figure 14: Refection of a planar shock by a wedge : density contours, second order solution. Min=1.4, Max=17.3. Contour from 1.4 to 19.088, $\Delta\rho = 0.36$
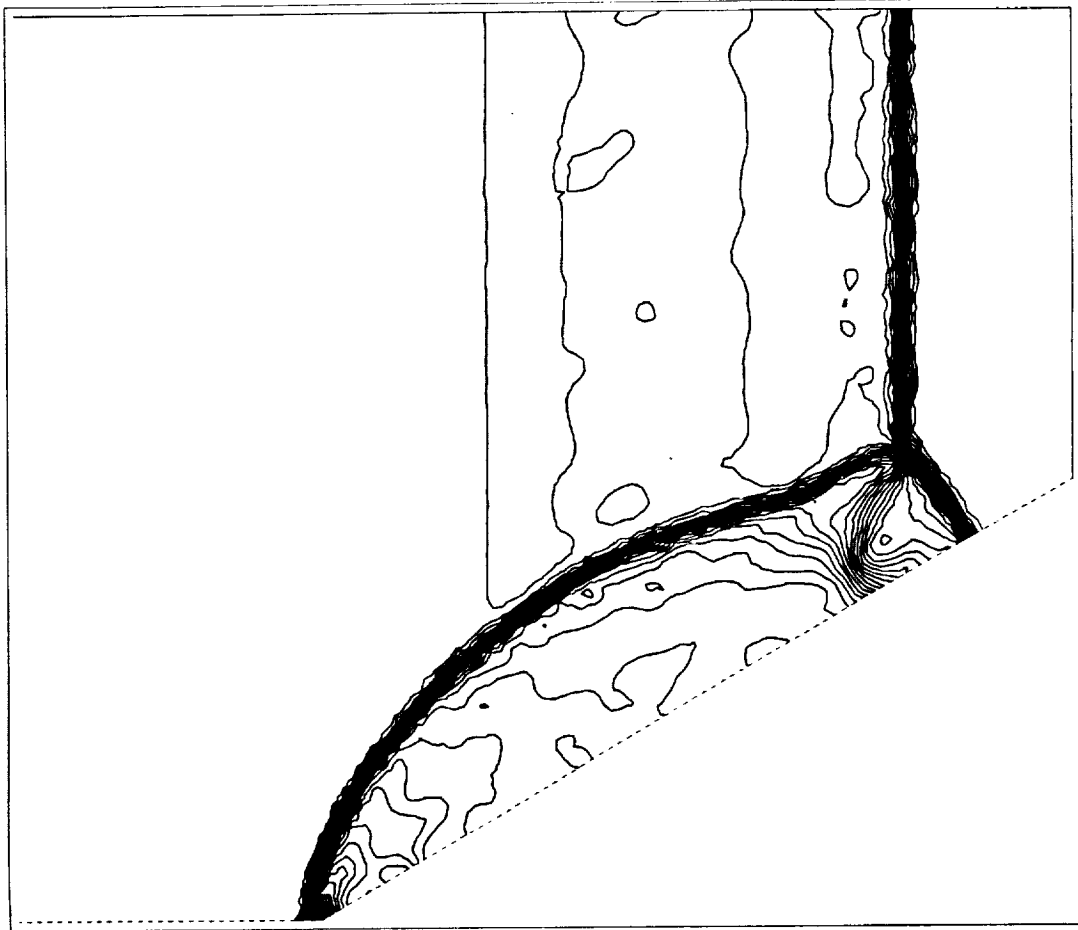
Figure 15: Refection of a planar shock by a wedge : density contours, third order solution. Min=1.4, Max=19.088, $\Delta\rho = 0.36$

REPORT DOCUMENTATION PAGE

Public reporting burden for this collection of information is estimated to average 1 hour per response, including the time for reviewing instructions, searching existing data sources, gathering and maintaining the data needed, and completing and reviewing the collection of information. Send comments regarding this burden estimate or any other aspect of this collection of information, including suggestions for reducing this burden, to Washington Headquarters Services, Directorate for Information Operations and Reports, 1215 Jefferson Davis Highway, Suite 1204, Arlington, VA 22202-4302, and to the Office of Management and Budget, Paperwork Reduction Project (0704-0188), Washington, DC 20503

1. AGENCY USE ONLY (Leave blank)	2. REPORT DATE December 1992	3. REPORT TYPE AND DATES COVERED Contractor Report

4. TITLE AND SUBTITLE ON ESSENTIALLY NON-OSCILLATORY SCHEMES ON UNSTRUCTURED MESHES: ANALYSIS AND IMPLEMENTATION	5. FUNDING NUMBERS C NAS1-19480 WU 505-90-52-01
6. AUTHOR(S) R. Abgrall	

7. PERFORMING ORGANIZATION NAME(S) AND ADDRESS(ES) Institute for Computer Applications in Science and Engineering Mail Stop 132C, NASA Langley Research Center Hampton, VA 23681-0001	8. PERFORMING ORGANIZATION REPORT NUMBER ICASE Report No. 92-74

9. SPONSORING/MONITORING AGENCY NAME(S) AND ADDRESS(ES) National Aeronautics and Space Administration Langley Research Center Hampton, VA 23681-0001	10. SPONSORING/MONITORING AGENCY REPORT NUMBER NASA CR-191415 ICASE Report No. 92-74

11. SUPPLEMENTARY NOTES
Langley Technical Monitor: Michael F. Card   Submitted to Journal of Final Report   Computational Physics

12a. DISTRIBUTION/AVAILABILITY STATEMENT Unclassified - Unlimited Subject Category 34,64	12b. DISTRIBUTION CODE

13. ABSTRACT (Maximum 200 words)

A few years ago, the class of Essentially Non-Oscillatory Schemes for the numerical simulation of hyperbolic equations and systems was constructed. Since then, some extensions have been made to multidimensional simulations of compressible flows, mainly in the context of very regular structured meshes. In this paper, we first recall and improve the results of an earlier paper about non-oscillatory reconstruction on unstructured meshes, emphasising the effective calculation of the reconstruction. Then we describe a class of numerical schemes on unstructured meshes and give some applications for its third order version. This demonstrates that a higher order of accuracy is indeed obtained, even on very irregular meshes.

14. SUBJECT TERMS ENO Schemes, high order accuracy, numerical shock capturing scheme, unstructured meshes	15. NUMBER OF PAGES 37
	16. PRICE CODE A03

17. SECURITY CLASSIFICATION OF REPORT Unclassified	18. SECURITY CLASSIFICATION OF THIS PAGE Unclassified	19. SECURITY CLASSIFICATION OF ABSTRACT	20. LIMITATION OF ABSTRACT